PCCP

Accepted Manuscript

ROYAL SOCIETY OF CHEMISTRY

www.rsc.org/pccp

Suspensions of carbon nanofibers in organic medium: Rheo-electrical properties

Mohamed Youssry[a*], Dominique Guyomard[b], Bernard Lestriez[b*]

[a] Department of Chemistry and Earth Sciences, College of Arts and Sciences, Qatar University, 2713 Doha, Qatar

[b] Institut des Matériaux Jean Rouxel, CNRS, Université de Nantes, 44322 Nantes Cedex 3, France

*Corresponding authors:
Mohamed Youssry (myoussry@qu.edu.qa)

Abstract

The nonaqueous suspensions of carbon nanofibers (CNFs) in 1 M lithium bis(trifluoromethanesulfonaimide) in propylene carbonate electrolyte reveal unique structural evolution and shear-induced transition due to the high aspect ratio. The rheo-electrical behavior elucidates a microstructural transition from entangled-to-aggregated networks above a distinct percolation threshold. Under shear flow, both networks show three-regime flow curve and inverted-bell-like conductivity curve as a consequence of shear-induced alignment (entangled network) and shear-induced breaking up (aggregated network).

The different particle morphology of carbon nanofibers (anisometric) and carbon black (CB; isometric) causes different aggregation mechanisms (aggregated vs. particulate) and then varied microstructure for their suspensions in the same electrolyte. This fact explains the higher rigidity and lower electric conductivity of CNFs than CB suspensions. Interestingly, the suspension of hybrid carbons at optimum mixing ratio merges the advantages of both carbons to operate efficiently as precursor in the formulation of electrodes for energy storage systems.

Keywords

Carbon nanofibers; rheo-electrical properties, suspension in organic medium, mixed carbon suspensions.

1. Introduction

Carbon nanofibers (CNFs) are special kind of carbonaceous nanomaterials which have been widely used a conductive filler in the formulations of electrodes for energy storage systems such as ion-batteries[1-6] and electrochemical capacitors[7], due to their unique chemical, mechanical, and electrical properties. They resemble carbon nanotubes (CNTs) where both nanomaterials are formed from graphite sheets with sp^2 hybridized carbon atoms arranged in cylindrical structure, while the sheets are stacked with an angle to the fiber axis (not parallel) resulting in exposed edge planes on the interior and exterior surfaces of the nanofibers.[8] According to the feedstock, synthesis route and conditions, CNFs have wide range of aspect ratios (length/diameter>100) with an average diameter of 50-200 nm and length scale of several tens of μm.[9] Such high aspect ratio and strong van der Waals attraction forces result in aggregation (bundling) of nanofibers and formation of larger agglomerates so that flocculated suspensions are formed especially at higher CNF concentration in polar solvents, similar to CNTs suspensions.[10] The electric current only flows on the outermost fibers in a bundled CNFs, while the inner fibers do not contribute significantly to the current[11] resulting in potential loss of electronic wiring. To overcome the dominant van der Waals forces, many approaches, including physical adsorption of amphiphiles[12,13] and chemical functionalization[14,15], have been developed and stable dispersions of such filamentous materials (CNTs or CNFs) have been obtained. However, these methods seriously disrupt the graphitic structure of the sidewall[16] and reduce the aspect ratio[17] of nanofibers/nanotubes resulting in a significant change in the electrical conductivity of suspensions. Moreover, the colloidal stability of the suspensions becomes out of control when the nanofibers/nanotubes entangle and then percolate far above a critical concentration, the so-called *percolation threshold* (ϕ^*; ϕ denotes the volume fraction of carbon materials). Above this threshold, two- or three-dimensional network of nanofibers/nanotubes is formed which is signified by an abrupt change in the rheological parameters (plateau modulus G_0 or yield stress σ_y)[18] when the infinite network is constructed. This is called the rheological percolation threshold (ϕ_r^*). On the other hand, the electrical percolation threshold (ϕ_e^*) is characterized by a sudden increase in the electrical conductivity (Σ) when the conductive pathways are formed across the suspension. Usually, the rheological and electrical thresholds slightly differ and in some cases coincide depending on the state of dispersion, particles orientation and size distribution.[19,20] In

general, even small infinite cluster is required to reach the electrical threshold; however, the rheological threshold appears when a three-dimensional rigid network is fully formed.[20]

In comparison to low-aspect-ratio (nearly isometric) particles such as carbon blacks (CBs), anisometric particles such as CNTs and CNFs are expected to: (i) reach the percolation thresholds at concentrations lower than those of isometric particles such as carbon blacks (CBs)[19,21], (ii) have different agglomeration mechanism, and (iii) respond differently to shear flow. For instance, it is known that the percolating network of aggregated suspension of CBs suffers shear-induced transition under simple shear flow as a consequence of the breaking up of aggregates into smaller flocs.[5] Owing to their higher aspect ratio and flexibility, nanofibers are likely to resist the breaking up of the network, to some extent, so that conductive clusters exist yet.

Carbonaceous materials such as carbon nanofibers are essential conductive component in electrodes formulation for battery applications. In order to improve the energy density of battery, the amount of active material (which is electrically insulator) should be increased. This increase breaks up the electrically percolating network resulting in electrical pathways loss.[6,22] Beside their excellent electrical properties, the filamentous morphology and flexibility of carbon nanofibers adapt them to be used as a conductive component which sustains higher loading of active materials and shear-induced breaking up of their network. Vapor grown carbon fibers are special type of carbon fibers which are characterized by large surface area, small diameter, high mechanical strength, electrical conductivity, and unique network-like morphology; thus they showed improved performance in the electrodes of lithium-ion batteries.[3]

In this work, we have systematically studied the flow-structure relationship in suspensions of carbon nanofibers in organic electrolyte (1 M lithium bis(trifluoromethanesulfonaimide) in propylene carbonate) for redox-flow batteries at 25 °C. Under the same conditions, the effect of particle morphology (isotropic carbon black vs. anisometric carbon nanofiber) on the equilibrium agglomeration mechanism and shear-induced transition is comparatively addressed. In addition, the rheo-electrical behavior of suspensions of mixed carbons (carbon black and nanofibers) is demonstrated in attempt to find out optimum composition of conductive suspension as a precursor for electrodes for battery applications.

2. Experimental

2.1. Materials and suspensions preparation:

Carbon nanofibers (CNFs; Vapor-Grown Carbon Fiber-S with an average diameter d=100 nm, average length L=10 μm, density=1.90 g.cm^{-3}, and BET surface area=35 m^2.g^{-1}) and propylene carbonate (PC; 99.7%) were purchased from Showa Denko and Sigma-Aldrich, respectively. Lithium bis(trifluoromethanesulfonaimide) (LiTFSI) was kindly provided by 3M as a gift.

Using ball-milling (FRITSCH, Planetary Micro Mill PULVERISETTE 7 classic line), the suspensions were prepared by mixing appropriate amounts of CNF with solution of 1 M LiTFSI in propylene carbonate for 3 h at the ambient temperature. As recommended by FRITSCH, 12-mL grinding bowls were used to commonly prepare 5 mL suspensions. This preparation method yielded homogeneous suspensions with reproducible data.

2.2. Rheo-electrical measurements:

Simultaneous electrochemical impedance spectroscopy (EIS) measurements under shear flow were conducted in stress-controlled rheometer Physica MCR 101 (Anton Paar) equipped with a steel plate-plate geometry (plate diameter 50 mm, gap 1 mm) connected with a standard potentiostat/galvanostat (SP200 from Biologic, France). The plate-plate gap was 1 mm; hundred times larger than the fiber length to eliminate any effect of measurement boundaries.[23]

After loading the suspensions, the shear history was removed by preshearing the samples at 1000 s^{-1} for 10 min and left at rest for 1 h before sweeping the shear rate. At each shear rate, the rheological and electrical data were collected after 30-60 min, depending on the shear rate, where the steady state conditions were attained. The EIS spectra were measured over a frequency range of 10^{-2}-10^5 Hz at 25 °C with alternating current amplitude of 100 mV.

In this study, the electronic conductivity (Σ) values have been obtained by fitting the impedance spectra (see Nyquist plots; Fig. 5) of the samples to an equivalent circuit proposed in our previous study[5] and EC-Labs software (Bio-Logic Science-Instruments). The migration of the ions is described by an ionic resistor associated in serial with a capacitive element to take into account the accumulation of ions at the surface of the electrodes compensating their

polarization, known as the double-layer. The circulation of the electrons through the percolating network of CB is described by a pure electronic resistance Re in parallel with the ionic branch.

2.3. Electron Microscopy:

The scanning electronic microscope (SEM) JEOL JSM 7600F equipped with energy-dispersive X-ray (EDX) analyzer, operating in secondary electrons (SEI) mode was used to collect the samples' micrographs. After sample preparation, suspension was placed on the sample holder and left to dry before coating with thin layer of platinum. On the other hand, the morphology of the carbon nanofibers was investigated by transmission electron microscopy (TEM). The TEM specimen was prepared by dispersing traces of CNF powder in acetone; a drop of dispersion was applied to a grid and then dried in air before TEM experiments.

3. Results and discussion

3.1 Morphology of carbon nanofibers

Generally, vapor grown carbon nanofibers are unique kind of carbonaceous materials that have high aspect ratio (L/d), with large diameter in between carbon nanotubes and conventional nanofibers.[24] In the current study, we use a vapor grown carbon nanofibers with diameter d= 100 nm and average length L=10 μm, so that the aspect ratio (L/d) = 100. As can be seen from TEM micrographs (Figs. 1a,b), the nanofibers have a tree-ring structure with a hollow core and semispherical tip. Moreover, the nanofibers contain bends and other curvatures, and some have bamboo-like structure with the distance between joints of about 500 nm. Most of the nanofibers are not perfectly straight, leading to structurally weak points, i.e. more flexible nanofibers. The SEM micrographs represent the microstructure of the suspension of CNFs in propylene carbonate (PC) in presence of LiTFSI as a salt. High-magnification SEM micrograph (Fig. 1c) shows highly entangled nanofibers which are bundled into large aggregates (bundles) of few tens of μm in diameter (Fig. 1d). The aggregates are linked by nanofibers forming an interconnected three dimensional network (Fig. 1d). This is the role of LiTFSI salt which is likely to electrostatically stabilize the aggregates so that a homogenous distribution of connected bundles are formed when compared to the salt-free suspension which shows relatively larger isolated bundles (Fig. S-1 in supplementary data).

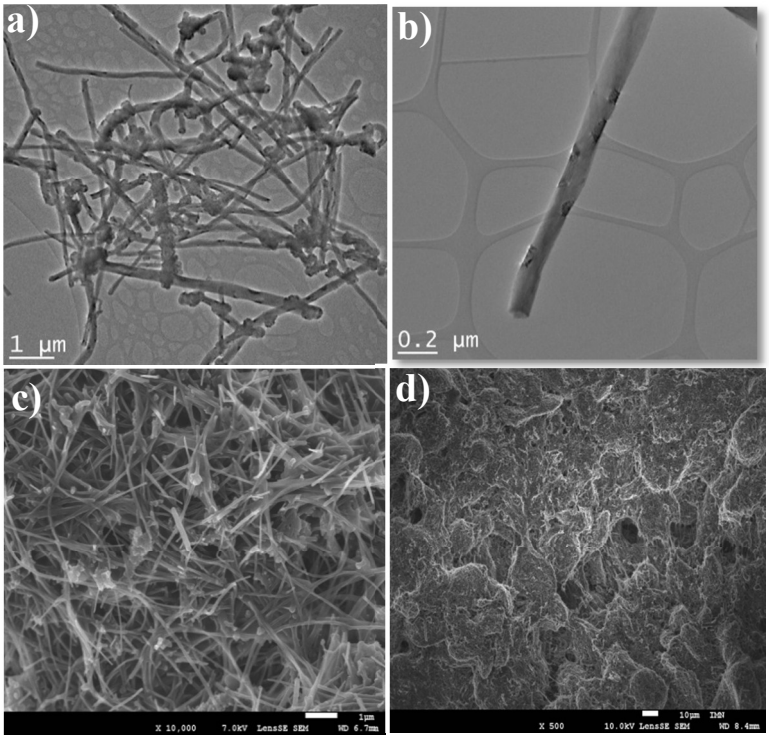

Fig. 1. TEM (a,b) and SEM (c,d) micrographs of CNFs (the bars in micrographs c and d correspond to 1 and 10 µm, respectively).

3.2. Nonlinear viscoelasticity of CNFs suspensions

Beside its usage to define the linear viscoelastic regime, strain sweep measurement is used to explore the flow behavior of suspensions under large deformation. For some selected suspensions, Fig. 2a shows the strain sweep curves; variation of the elastic (G') and viscous (G'') moduli as functions of the maximum applied oscillatory strain (γ). Rationally, the magnitude of dynamic moduli monotonically increases with the CNFs concentration. At small strains, G' is always higher than G'' and suspensions behave gel-like until a critical strain (γ_c) beyond which the moduli crossover appears then G'' becomes higher than G' where the suspensions are liquid-like. For the diluted suspensions, however, it can be noticed that G'' initially rises and then decreases exhibiting a strain overshoot[25] before the moduli crossover and the suspensions behave strain weakening. Such behavior has been reported previously for soft materials[26] and CNTs suspensions[27,28] which was attributed to the formation of a transient weak structure which resists the deformation then breaks up above a critical strain (γ_c).[26]

This strain overshoot diminishes as the CNFs concentration increases, and the critical strain shows a concentration dependence (Fig. 2b) represented by a power law relation with an exponent of -0.4 similar to that exhibited by networks of semiflexible polymers[29,30] and long

carbon nanotubes[31] where the deformation is likely attributed to the breaking of bonds between rods and network reorganization.[28,30]

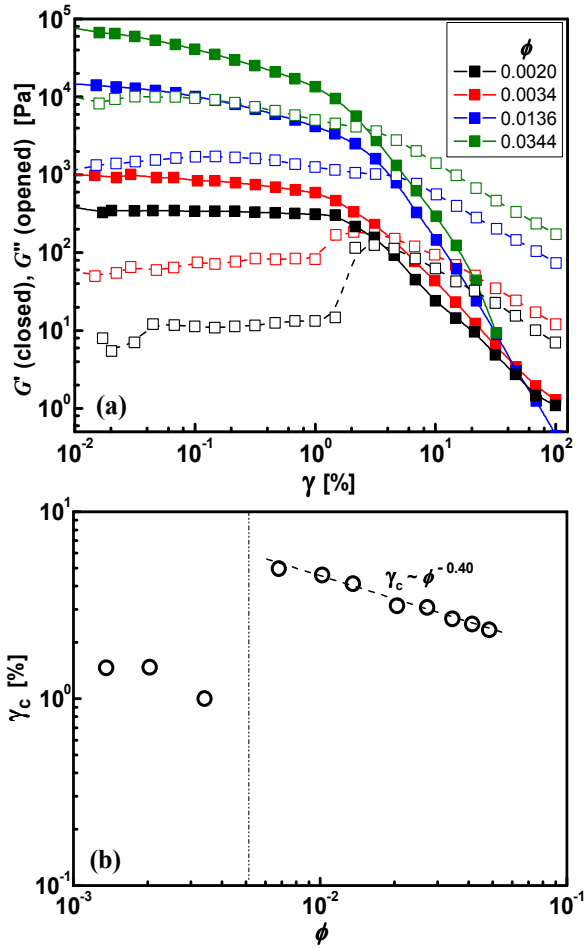

Fig. 2. (a) Strain amplitude dependence (at 1 Hz) of elastic G' (closed) and loss G'' (opened) moduli for some chosen suspensions, and (b) dependence of the critical strain (γ_c) on the nanofiber concentration.

Also, it is worth noting that the γ_c-ϕ curve (Fig. 2b) shows two regimes: at low concentration γ_c is almost independent of ϕ, then shows power law with negative exponent (-0.40) at higher concentration. This may implies a structural transition towards rigidly structured suspensions which are more sensitive to the strain as the CNFs concentration increases.

3.3.Linear viscoelasticity of CNFs suspensions

Insight into microstructure of CNFs suspensions, at equilibrium, can be obtained from the frequency sweep measurements at small deformation in the linear viscoelastic regime in order to guarantee the least disturbance of the internal structures. Dynamic rheological measurements

were performed on a wide range of CNFs concentration where typical curves of the oscillating frequency dependence of G' and G'' are demonstrated in Fig. 3a. The suspensions exhibit a common gel-like behavior where G' is one-decade higher than G'' and both moduli are nearly independent of the frequency over the entire range. The viscous modulus G'' of the diluted suspension varies slightly with the frequency until G'-G'' crossover appears at higher frequency. This implies the weak gel-like nature of the diluted suspensions. As the CNFs concentration increases, the suspensions turn into strong gel-like where the moduli are completely independent of the frequency and hence the moduli crossovers disappear. This viscoelastic behavior denotes strongly flocculated suspensions with dominant strong irreversible attraction forces (involving energies of several hundreds of kT units).[32] Such behavior has been previously reported for suspensions of spherical carbon black in dispersing medium with poor affinity towards the dispersing particles[5,33,34] and concentrated carbon nanotubes suspensions.[27,28,35-37]

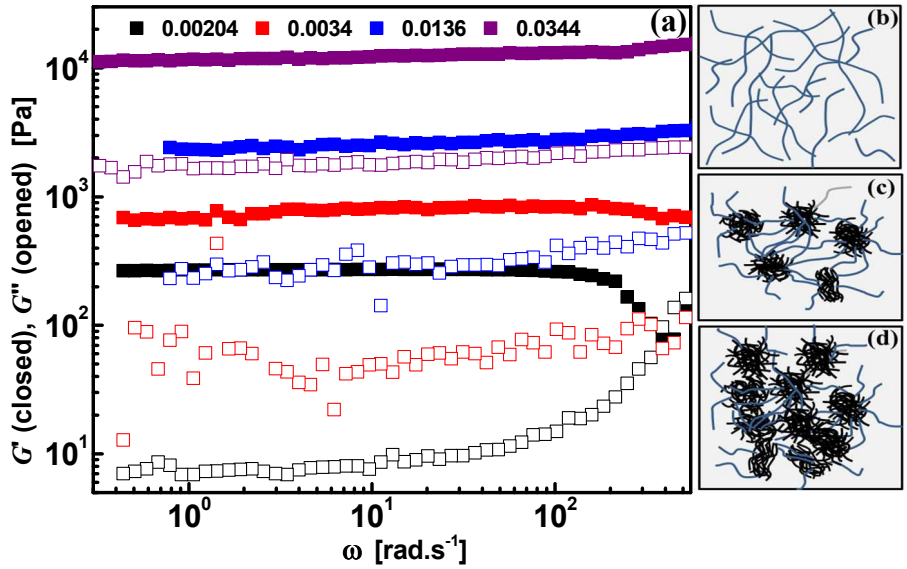

Fig. 3 (a) Dynamic frequency sweep of CNFs suspensions at 25 °C. The strain amplitude values, at the linear viscoelastic regimes, were chosen 0.3 – 1 % depending on the strain sweep. (b-c) schematic representation for possible network structure.

For carbon nanotube suspensions, Hough et al attributed the network elasticity to the formation of interconnected networks with bonds that freely rotate and resist stretching.[28] Analogously, it is rational to ascribe the viscoelasticity of the CNFs suspensions, at moderate concentration, to the formation of a three-dimensional network formed from aggregates (bundles) held together by freely jointed fibers as schematically represented in Fig. 3c and suggested from SEM micrograph (Fig. 1 d). This network becomes densely packed (Fig. 3d) as

the volume fraction of nanofiber increases (as will be described below). For an analogous system (CNFs suspension in glycerol/water), Xu et al demonstrated the strong tendency of CNFs to clump into mm-sized showing gel-like behavior at higher concentration.[38]

It is well stated that suspensions of high-aspect-ratio rods are not dilute unless their volume fraction is very low, $\phi \leq (L/d)^{-2}$.[39] Accordingly, it is expected to have CNFs suspensions in the semidilute regime at $\phi \geq 0.0001$ (with aspect ratio =100) if they are well dispersed. This is the behavior of the suspensions at low concentration (ϕ = 0.0014-0.0034) which exhibit a gel-like viscoelastic response with $G' > G''$ in contrast to many colloidal systems that showed liquid-like response at similar concentrations.[35,37,38,40,41] Such behavior has been reported previously for very dilute CNTs suspensions.[27,28] Hough et al reported a rigidity percolation transition in surfactant–stabilized suspensions of single wall CNTs (aspect ratio≈150) at ϕ=0.0026.[28] It is presumably the entangled network of carbon nanofibers (Fig. 3b) that is responsible for such weak gel-like viscoelastic behavior even at very low concentration. Therefore, the microstructural transition and precision determination of thresholds can be followed by examining the variation of the rheological parameters with the concentration of nanofibers.

The plateau modulus (G_0) and yield stress (σ_y) are two important rheological parameters which stand for the network rigidity in terms of number and lifetime of physical bonds between aggregates and the development of network size and compactness. Figures 4a and b depict the variations of G_0 and σ_y with the volume fraction of nanofibers (ϕ) which are represented by power law relations: $G_0 \sim \phi^m$ and $\sigma_y \sim \phi^n$ with three distinct exponents for m and n correspond to three distinct regimes (Table 1). As mentioned above the diluted suspensions ($\phi \leq 0.0068$) are gel-like viscoelastic with considerable G_0 which shows minor dependence (m=0.69) of ϕ implying a constant entanglement density of individual nanofibers analogous to semiflexible biopolymers.[43] At $\phi > 0.0068$, G_0 and σ_y steeply increases exhibiting power law relationship with exponents: m=2.1 and n=1.8, respectively. Generally, these exponents are very close to that reported for suspensions of anisometric particles such as CNTs[27,28,31,35,44] and semiflexible biopolymer[29,43] forming a three-dimensional network with bonds resisting stretching and free to rotate.[28] The highly concentrated suspensions ($\phi > 0.034$) show higher exponent m=6.3 and n=6.9, similar to that reported for short single-walled CNT (aspect ratio=80) at similar concentration,[31] and multi-wall CNT suspensions in polydimethylsolixane (aspect ratio=160).[44]

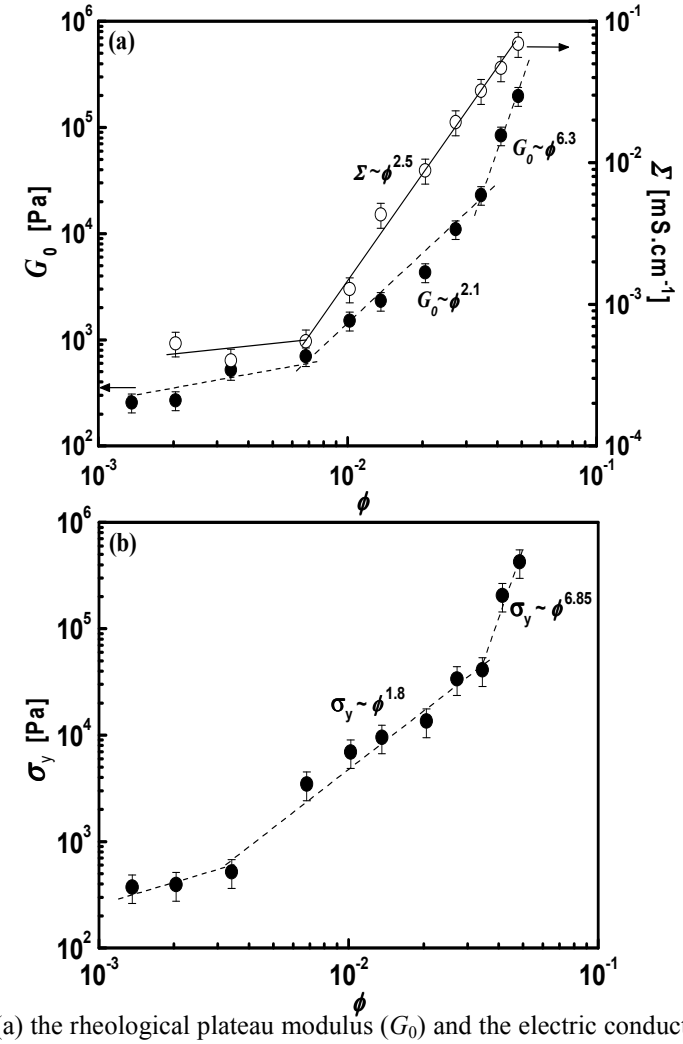

Fig. 4 Variation of (a) the rheological plateau modulus (G_0) and the electric conductivity (Σ), and (b) the yield stress (σ_y) with the concentration of CNFs. The lines are the best fit. The yield stress was calculated using the relation: $\sigma_y=G_0\gamma_c$.[26,42] The electric conductivity was obtained by fitting the impedance spectra to the equivalent circuit (inset of Fig. 5) and substituting Re in the equation: $Re=e/\Sigma S$ where e is the thickness of the suspension (gap between upper and lower plate in the rheo-dielectrical cell), S the plates surface.

Table 1. The evolution of the exponents m (for $G_0\sim\phi^m$) and n (for $\sigma_y\sim\phi^n$) and the estimated fractal dimensions (D^* and D^{**} denote the values estimated, respectively, using m and n) with the concentration of nanofibers. The critical volume fractions of the I-to-II and II-to-III transitions are, respectively, 0.0068 and 0.034.

	m	n	D^*	D^{**}
Regime I: Entangled network	--	--	--	--
Regime II: aggregated network (strong-link regime)	2.1	1.8	--	1.9
Regime III: aggregated network (weak-link regime)	6.3	6.9	2.8	2.7

This behavior is likely to ascribe to a structural transition from entangled (non-aggregated) network to aggregate-based network above the rheological percolation threshold (ϕ_r*=0.0068). This latter network is considered to have a fractal nature where the aggregates (flocs) are closely packed throughout the sample. This fractal nature is related to the dependency of the rheological

parameters G_0 and σ_y on the nanofiber concentration where two behaviors can be distinguished-depending on the strength of the interfloc links in comparison to that of the flocs (intrafloc) in three-dimensional network: strong-link behavior (Eq. 1) and weak-link behavior (Eq. 2):[45,46]

$$G_0 \sim \phi^{(3+x)/(3-D)} \quad (1)$$

$$G_0 \sim \phi^{1/(3-D)} \quad (2)$$

where D is the fractal dimension of the flocs and x is the backbone fractal dimension of the flocs. In the strong-link regime, the interfloc links are stronger than the intrafloc links at low ϕ and the macroscopic elasticity is dominated by intralinks.[45,46] In this regime, the fractal dimension D cannot be calculated using the power-law exponent of G_0 predicted by Shih model (Eq. 1) due to the unusual negative value of x.[47] Alternatively, D is calculated from the power law exponent of σ_y:[48,49]

$$\sigma_y \sim \phi^{2/(3-D)} \quad (3)$$

and was found to be 1.9 in accordance with the scaling model in the strong-link regime of flocculated suspensions.[45,46,50,51] This fractal dimension implies a fast aggregation when the flocs grow by merging into one another as soon as they colloid (diffusion-limited aggregation, DLA[52,53]). As the nanofiber concentration increases, the suspensions are in the weak-link regime where the flocs are more rigid than the interfloc links so that the macroscopic elasticity of the interfloc links determines the elasticity of the suspensions.[45,46] The scaling relations of G_0 and σ_y (Eqs. 2 and 3) show almost similar fractal dimension D=2.7-2.8 in an excellent agreement with the predict value in the weak-link regime.[46] This implies a different aggregation mechanism (reaction-limited aggregation, RLA) where the flocs penetrate to one another partially after collision[39] and more compact structure[32] is formed in highly concentrated suspensions.

In conclusion, the CNFs suspensions, below the rheological percolation threshold, are self-similar entangled network that cannot be explained from the framework of fractal network.[44] At the percolation threshold (ϕ_r*=0.0068), they exhibit a transition from DLA (D=1.9) to RLA (D=2.7) as the concentration increases in agreement with previous findings.[51] Such transition is in line with microstructural evolution of the aggregated suspensions that are large flocs linked by fibers (strong-link regime) and transform to densely-packed (compact) network of more rigid flocs at higher concentration.

3.4. Electrical properties of CNFs suspensions

Simultaneous measurements for the electric conductivity of the suspensions at no perturbation (after the dynamic frequency sweep) proved to be an efficient way to eliminate any additional stress and produce consistent interpretation for the microstructure of suspensions under investigation.[5,6] The degree of particles' agglomeration, extent of conductive pathways through the network and the electrical resistance of the gaps between particles/aggregates are reflected by the electric conductivity of the suspensions (Σ). Figure 5 represents the variation of the impedance spectra (Fig. 5) with the volume fraction of CNFs. It can be seen that the dilute suspensions show nearly linear Nyquist plot similar to that of the electrolyte (1 M LiTFSI in PC) implying the ionic nature of the suspensions. As the CNFs concentration increases, typical semicircle Nyquist plots start to appear above a concentration threshold, the so-called electrical percolation threshold ϕ_e^*, indicating the build-up of the conductive network. This transition has been previously found in carbon black suspensions in the same electrolyte.[5]

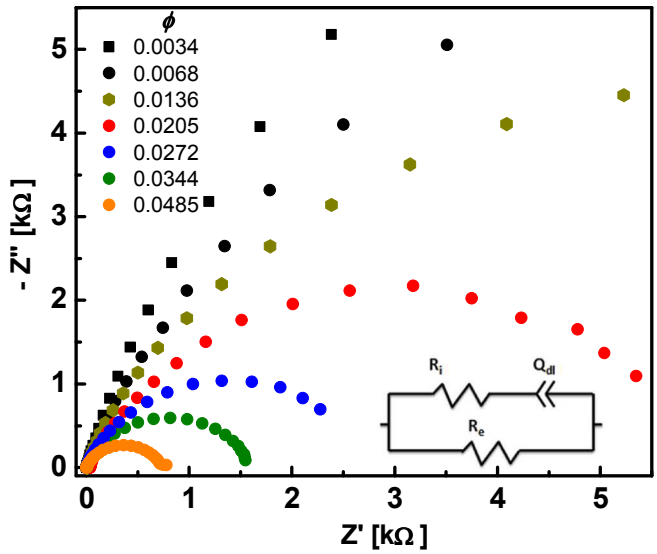

Fig. 5 Impedance spectra represented by Nyquist plots for CNFs suspensions at various CNF concentrations (at 25 °C, 100 mV) measured in plate-plate geometry with a plate diameter of 50 mm and gap of 1 mm. The equivalent circuit used in the analysis is superimposed on the Nyquist plot. The migration of the ions is described by an ionic resistor R_i associated in serial with a capacitive element Q_{dl} to take into account the accumulation of ions at the surface of the electrodes compensating their polarization, known as the double-layer. The part of the circuit corresponding to the presence of nanofibers is placed in parallel with the ionic branch. It is constituted of a pure electronic resistance R_e to take into account the circulation of the electrons through the percolating network.[5]

Figure 4a shows a quantitative variation of the electric conductivity with the volume fraction of CNFs. At low ϕ, the electric conductivity is nearly constant until the percolation threshold beyond which the electric conductivity sharply increases exhibiting a power-law relation:

$$\Sigma \sim \phi^{l} \tag{4}$$

with an exponent l= 2.5. This exponent is in agreement with the theoretical one (l=2) reported for three-dimensional percolating network[54] and experimental values (l=2.2 and 2.3) found in CNT/polymer nanocomposites[55-58] and 3D network of carbon black suspensions.[5]

Surprisingly, the electrical percolation threshold (ϕ_e^*) coincides with the rheological threshold at a volume fraction of 0.0068. Some CNT/polymer nanocomposites showed coincidence thresholds[59-61] in contrast to the common behavior of flocculated suspensions where $\phi_e^* > \phi_r^*$.[55,56,62,63] It is well stated that the electrical percolation threshold is reached when the fibers approach each other with few nm resulting in a conductive pathways across the network. Therefore, the required fiber-fiber distance for electrical conductivity percolation is smaller than that for the rheological percolation, so that less nanofiber is required to reach the electrical conductivity threshold.[55] This is the situation for the entangled network of the nanofibers before the percolation threshold (0.0068) above which a *superstructure* of aggregate-based network formed from aggregates (flocs) linked by nanofibers such that the conductive pathways are dominated. As the concentration increases, the flocs get densely packed leading to higher electrical conductivity. This trend is in accordance with the dynamic rheological data. However, the rheological behavior of the suspensions is likely to be more sensitive to the structural transition than their electrical behavior: the variation of the rheological parameters G_0 and σ_y (Figs. 4a and b) with ϕ presents two inflection points at ϕ= 0.0068 and 0.034, correspond to a structural transition from open fractal structure to densely-packed one.

In this study, we define the percolation threshold (ϕ=0.0068) to be the volume fraction of CNFs at which the transition from entangled to superstructure (aggregate-based) network occurs. However, even the entangled network possess conductive pathways at ϕ=0.00204 in accordance with CNTs.[61,64] In general, the flocculated suspensions commonly showed varied percolation thresholds and scaling exponents as a consequence of formation process, particle size, interparticle interactions,[65,66] dispersing medium,[67] aspect ratio, and external stress (e.g. applied voltage).[61,62]

3.5. Steady shear rheology of CNFs suspensions

The dynamic viscoelasticity and the simultaneous impedance spectra at rest revealed the development of microstructure of suspensions with the concentration of the CNFs, at nearly no perturbation. Then, it is necessary to examine the effect of continuous shear flow on the microstructure of suspensions and account for any possible shear-induced structure/alignments in the internal structure.

Figures 6 demonstrate the flow curves (steady shear viscosity η or shear stress σ versus the applied shear rate $\dot{\gamma}$), and a comparison between the dynamic complex viscosity η* with the steady shear viscosity. First, the steady viscosity η increases with the concentration of nanofibers.[68] The suspension at low concentration (ϕ=0.00136) exhibits a monotonic non-Newtonian shear-thinning behavior over the entire shear rate (Fig. 6a) in accordance with flocculated colloidal suspensions of CNFs[38] and CNTs.[31,36,40,41,69] Interestingly, the suspensions at $\phi \geq 0.00204$ show a three-regime flow curve: two shear-thinning regions at low and high shear rates separated by a shear-thickening (or plateau) region over intermediate shear rates (Figs. 6a and b). On sweeping the shear rate forward and backward a minor hysteresis appears indicating the reversibility of shear thickening. The thickening region is modest at low concentration and becomes pronounced and shifts to higher shear rate as the CNFs concentration increases. Such behavior has been found in suspensions of spherical colloids[5,70] and anisometric CNT.[69,71]

In general, the low-shear rate viscosity (before the thickening region) obeys a power-law expression: $\eta \sim \dot{\gamma}^{-1.0}$, with common exponent identical to the theoretical one[72] but independent of the CNFs concentration. According to the orientation/aggregation model,[72] the interparticle interactions, hydrodynamic forces and network elasticity are the controlling forces for the rheological behavior of suspensions under shear flow. The relative importance of each force is dependent on the shear rate and particle concentration. The dilute suspension (at ϕ=0.00136) is simple entangled network of nanofibers (no aggregates) that align individually in the flow direction as a consequence of network breaking up due to shear flow[41] showing shear thinning over the entire shear rate range. As the CNFs concentration increases, the network elasticity (due to agglomeration) and interparticle interactions become pronounced and the relative importance of each factor is concentration-dependent.[72] At low shear rate, the rod-rod interaction is dominant where the shear flow distorts the equilibrium isotropic orientation distribution of the fibers into anisotropic (ellipsoid) distribution[72] resulting in the shear-thinning (thinning I). On the

other hand, the hydrodynamic forces are dominant at higher shear rates[72] leading to higher degree of alignment of the nanofibers (thinning II).

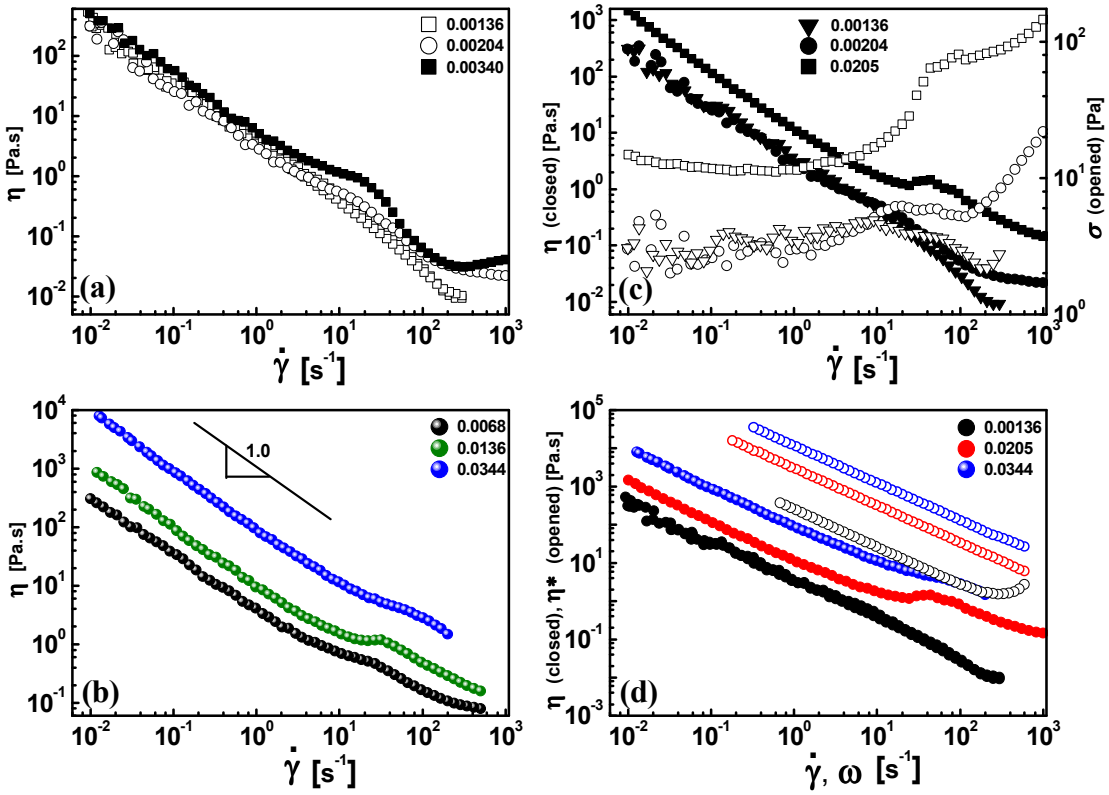

Fig. 6. Flow curves (a,b,c) and comparison between steady (η) and complex (|η*|) viscosity (d) for CNFs suspensions. The complex viscosity is extracted from the dynamic frequency sweep (linear) rheology.

The shear-thickening exhibited by the aggregate-based suspensions is likely to attribute to the formation of anisotropic aligned aggregates analogous to the hydroclusters formed in suspensions of spherical particles.[73,74] These anisotropic aggregates seem to erode resulting in higher effective volume fraction[75,76] and, hence, shear-thickening behavior at intermediate shear rates. Flow-induced agglomeration has been reported previously for CNTs suspensions.[77,78] Interestingly, the suspensions well below the percolation threshold also exhibit mild shear-thickening indicating the onset of aggregation formation but the percolating network has not established yet. The shear thickening can be viewed as a steep jump in the shear stress with increasing shear rate as shown in Fig. 6c. This jump is steeper for the percolating suspension (ϕ=0.0205) than for the non-percolating one (ϕ=0.00204) implying higher packing fraction of

eroded aggregates analogous to the densely packed suspensions and colloids.[79] However, the entanglements -based suspension (ϕ=0.00136) lacks the formation of anisotropic aggregates and only show monotonic shear-thinning consistent with leveling-off the shear stress over the entire shear rate range.

The effect of continuous shear flow on the microstructure of suspensions can be seen when comparing the steady viscosity (η) with the complex viscosity (|η*|) as depicted in Fig. 6d. For both diluted and concentrated suspensions, |η*| is one-decade higher than η at the same shear rate or frequency. This implies that the CNFs suspensions do not obey Cox-Mertz rule over the entire range of shear rate or frequency. Such behavior has been reported for suspensions of CNFs[38] and CNTs[41,69,80] when the network is established. Such deviation from Cox-Mertz rule (η<|η*|) is likely to be a consequence of the breaking of links between aggregates at equilibrium (initial) state due to continuous shear flow.

3.6. Rheo-electrical behavior of CNFs suspensions

Simultaneous measurements for the electric conductivity of the suspensions under continuous shear flow can elucidate the flow-induced structures or alignments that may be exhibited by the conductive suspensions of carbonaceous materials.[5,6,81]

The variation of the Nyquist plot shapes under shear flow is certainly a consequence of shear-induced structural transition. Therefore, it is necessary to quantitatively account for the variation of electric conductivity with the shear rates (Figure 7d), as will be discussed below. This figure displays the conductivities of percolating suspensions by fitting the semicircles only by the proposed equivalent circuit, while the linear plots not. Therefore, the rheo-electrical behavior of dilute and entangled suspensions will be discussed qualitatively.

In the quiescent state, the rheological and electrical behaviors of CNFs suspensions revealed a percolation threshold (ϕ=0.0068) that separates the entangled network from the percolating one. Far below this threshold, the diluted suspension at ϕ=0.00136 shows a clear linear Nyquist plot at rest (0 s^{-1}) which does not change upon shearing the sample (from 0.01 to 1000 s^{-1}) (Fig. S-3 in supplementary data). This suspension is pure ionic conductive and insensitive to the applied shear rate indicating minor degree of entanglement for this CNF (aspect ratio~100) suspension[31] and hence, it lacks electrical pathways. This suspension exhibits a monotonic shear-thinning without thickening region (Fig. 6a) implying the absence of any kind of agglomeration.

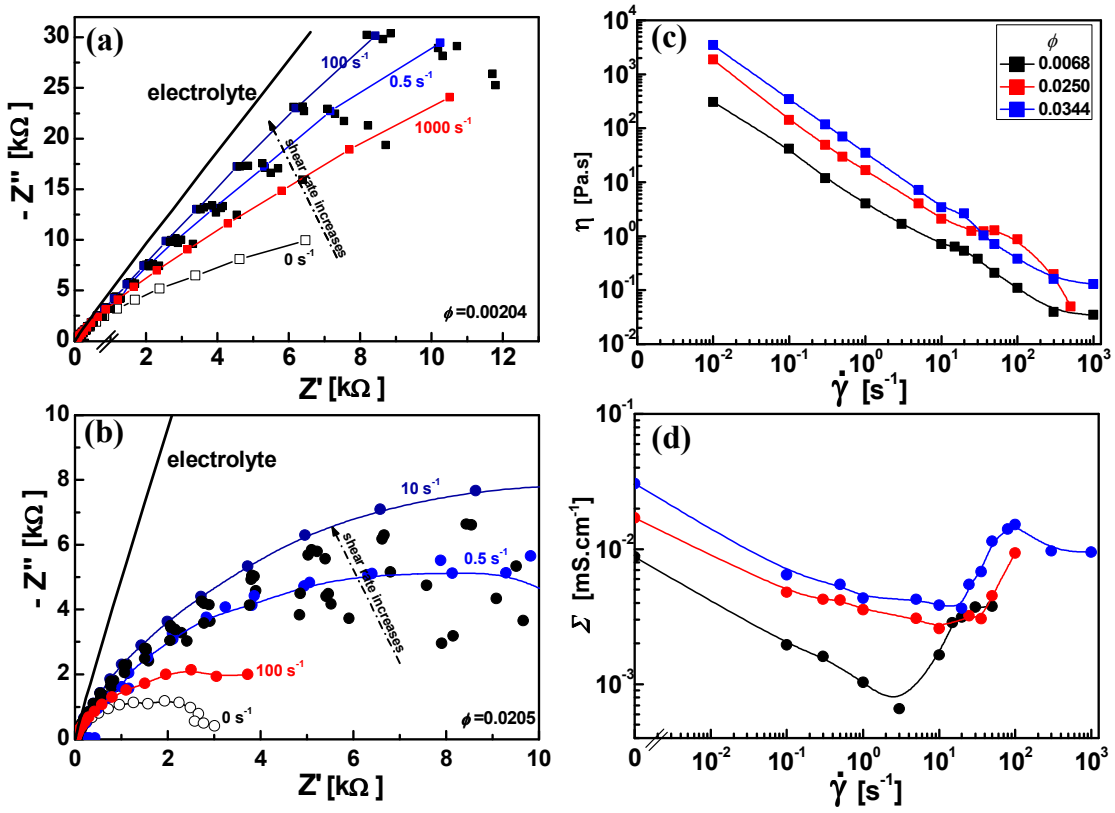

Fig. 7. The effect of shear rate on the electrical behavior of suspensions represented by Nyquist plots for (a) diluted suspension and (b) percolating suspension, and the variation of suspension's viscosity η (a) and electrical conductivity Σ (b) with the shear rate for percolating suspensions. Using the proposed equivalent circuit and EC-Labs software the semicircle plots *only* were fitted to obtain the conductivity values.

As the CNF concentration increases, the degree of entanglement become pronounced so that the entangled suspension at ϕ=0.00204 shows a nearly semicircle plot (Fig. 7a) implying the onset of the growth of electrical pathways. Upon shearing the suspension from 0.1 s^{-1} to 100 s^{-1} the nearly semicircle plot continuously transforms to linear plots until approaching the linear plot of the electrolyte implying that the suspension is no longer conductive. Above the critical shear rate (100 s^{-1}), the Nyquist plots surprisingly approach the nearly semicircle plot of the quiescent state at 1000 s^{-1} (Fig. 7a), i.e. the conductivity tends again to increase. The decrease in the conductivity (below 100 s^{-1}) is likely due to the breaking up of small aggregates and a reduction in the degree of entanglement while the nanofibers align in the flow direction[82] in tandem with the shear-thinning behavior discussed above. Above 100 s^{-1}, the shear-induce anisotropy causes an increase the conductivity in agreement with the behavior of CNT suspensions at high shear rate.[82]

On the other hand, the percolating suspension (ϕ=0.0205) shows typical semicircle Nyquist plot at rest (0 s^{-1}) which get progressively wider upon shearing the suspension from 0.1 s^{-1} until a critical shear rate at 10 s^{-1}. Beyond this critical value, the semicircles again get narrower until approach the semicircle of the suspension at rest (Fig. 7b). The simultaneous rheo-electrical behavior of the percolating suspensions is quantitatively depicted Figures 7 c and d. In general, the conductivity of suspensions at rest rationally increases with the CNF concentration. Upon shearing the suspensions, the conductivity drops in tandem with the first shear-thinning region (thinning I) indicating the destruction of the percolating network into smaller agglomerates. The conductivity drop becomes less steep as the CNF concentration increases as a consequence of strong rod-rod interaction and probably relatively large agglomerates that still *wire* the network. Above a critical shear rate (depending on ϕ), the conductivity again rises in consistence with the shear-thickening at higher intermediate shear rate as a result of the erosion between anisotropic aggregates that preserves the conductive pathways. At higher shear rate, the conductivity shows mild increase in accordance with the second shear-thinning region (thinning II) where the aggregates break up and the density of effective aligned nanofibers increases. It is worth noting that the conductivity minimum becomes less pronounced and shift to higher (critical) shear rate as the nanofiber concentration increases. This presumably is a consequence of larger shear-induced aggregations with considerable degree of anisotropy at higher CNF concentration.

Such inverted bell-like conductivity-shear rate curve has been reported for carbon black suspensions.[5] Various experimental[77,82,83] and numerical[84] studies on the conductivity of CNT/polymer suspensions under shear flow revealed the domination of aggregation mechanism at low shear rates and alignment mechanism at higher shear rates.

3.8. Comparison between CNF and CB suspensions and their mixture

The rheological and electrical properties of the suspensions of carbon materials were found to change with chemical properties and morphology of particles as well as the suspending medium.[5,85,86] Hence, it is worth to examine the effect of particle morphology (carbon nanofibers versus carbon black; KB) on the rheological and electrical properties of their suspensions in the same suspending medium (1 M LiTFSI in PC).

The rheo-electrical properties of KB suspensions in 1 M LiTFSI in PC over wide concentration range have been studied recently [5]. The KB suspensions showed a distinct transition from liquid-like ($G''>G'$) to weak-gel viscoelastic ($G'>G''$)[5] where the KB network began to be constructed at ϕ=0.002. This was defined as the rheological percolation threshold. Such transition is not obvious for CNFs suspensions which show gel-like response even at very low concentration due to their high aspect ratio. Therefore, the definition of rheological percolation threshold is varied and a quantitative comparison between the thresholds of KB and CNFs is not rational. However, it should be assumed that anisometric CNFs have lower rheological percolation threshold than isometric KB when the interconnected network is built up; i.e. when the viscoelastic behavior ($G'>G''$) appears. Comparatively, Figure S-4 in supplementary data depicts the variation of the rheological plateau modulus and electrical conductivity of CNFs and KB suspensions over wide concentration range. In general, the CNFs suspensions show a three-regime G_0–ϕ curve versus a monotonic increase of G_0 with the KB concentration (Fig. S-4a). This implies different mechanisms of structural evolution of CNFs and KB suspensions with the concentration. As described above, the CNFs exhibited a structural transition from entangled state to aggregated-based network which gets more compact as the nanofibers concentration increases. On the other hand, the KB suspensions are isolated agglomerates which grow with the KB concentration and eventually percolate.[5] Such different microstructure can be probed by following the power law exponents of $G_0 \sim \phi^m$, where m= 2.07 and 3.51 for CNFs and KB suspensions, respectively. These exponents are related to the fractal dimension D, where the

percolated CNFs show D=1.9 lower than that of percolated network of KB (D=2.5). Interestingly, these fractal dimensions indicate a common rapid (diffusion-limited) aggregation with aggregate-aggregate aggregation mechanism for CNF and particle-particle aggregation for KB suspensions.[32] The lower the value of D, the more open is the floc structure; and hence the CNFs are likely to form less compact network formed from large aggregates linked by nanofibers whereas, the relatively smaller KB aggregates form more dense network. Different aggregation mechanism and network compactness are consequence of different aspect ratios of the particles, where highly anisometric nanofibers (aspect ratio=100) might produce a network with less packing fraction than that of isometric spherical carbon black (aspect ratio=1) in accordance with the findings reported previously.[87]

Generally, the CNFs suspensions have G_0 higher than that of the KB suspensions. Below ϕ=0.0068 (the rheological percolation threshold of CNFs), the rigidity of highly entangled nanofibers is two-decade higher than that of loose and small KB aggregates. Above this concentration, G_0 of both suspensions approach each other when both suspensions are quite percolated. It is the aggregated-based microstructure in which the larger CNFs aggregates are linked by freely rotating nanofibers resulting in highly interacting flocs but still more open network than relatively smaller KB aggregates that form more compact structure. Such differentiation in the microstructure is reflected in the rheological plateau modulus where it is likely that the large aggregates and connecting bundles of nanofibers show higher rigidity than that of smaller aggregates linked by relatively weaker KB branches.

It should be noted that the electrical conductivity values of suspensions (CNFs or KB) were obtained by fitting the nearly or semicircle Nyquist plots by the proposed equivalent circuit in this study (see the caption of Fig. 5). As can be seen from Fig. S-5 in supplementary data, the suspensions show nearly semicircle Nyquist plots at ϕ=0.00204 for CNFs and ϕ=0.0034 for KB. They are the critical concentrations at which the insulating suspensions transform into electrically conductive ones when the conductive pathways begin to be built through the suspensions. Therefore, it is worth mentioned that the CNFs are electrically percolated at concentration nearly twice lower than that of KB. Similar to the rheological behavior, the electrical conductivity of the CNFs suspensions remains constant at low CNFs concentration then suddenly increases above an obvious electrical percolation threshold (ϕ_e*=0.0068) where the suspensions exhibit an entangled-to-aggregated transition (Fig. S-4b). However, the KB

suspensions do not show such an inflection point which separates the insulating and conducting suspensions. The carbon particles' morphology and perhaps different surface chemistry are likely to be the main factors which result in varied percolation thresholds and microstructural transitions. As the carbon concentration increases, the anisometric nanofibers show insulating-to-conductive-to-fully percolated network, in contrast to the isometric KB which exhibit insulating-to-percolated suspensions.

For the fully percolated KB and CNFs suspensions, the electrical conductivity shows a power-law relation: $\Sigma \sim \phi^{l}$, with different exponents: l=1.83 and 2.47 for KB and CNFs, respectively. These exponents fall in the theoretical range reported for 2D and ideal 3D networks[54], where l= 2.47 is consistent with a 3D network of aggregated CNFs while l=1.83 suggests KB arranged in 2D network.[5] This difference is likely attributed to the varied particle size and morphology where a denser network allows almost 2D conducting paths in agreement with the trend of the plateau modulus.

In contrast to the rheological behavior, CNFs suspensions are less conductive than the KB suspensions at the same conditions (Fig. S-4b). This behavior may be linked to different mechanisms of structural evolution between nanofibers and carbon black suspensions, where most of the electric current is lost in the inner fibers and the electric current only flows on the outermost fibers in bundled CNFs.[11]

4. Suspensions of mixed carbons

In addition to enhancing the mechanical properties of polymer-based composites, mixtures of carbonaceous materials (e.g. carbon black and nanotubes) have been used to increase the electrical conductivity of the composites.[88-90] Little research has been done in this area and we found a necessity to examine the effect of nanofibers on the rheo-electrical properties of carbon black suspensions. Figure 8 presents the rheo-electrical properties of examples of suspensions composed of varied mixtures of CNFs and KB at a total concentration fixed at 2 wt% (ϕ=0.0136). As can be seen from Fig. 8a, the replacement of up to 1 wt% KB by an equivalent amount of CNFs does not significantly alter the network rigidity but increases the electrical conductivity of the suspensions. Further increasing of the CNFs ratio results in increasing the rigidity and dramatically decreases the conductivity of the suspension. This behavior can be explained on the basis of the formation of co-supporting network[88,89] of

randomly distributed nanofibers and KB particulates where the nanofibers, at low content, act as long-distance wires and the particulate KB forms local conductive paths acting as interconnections between the nanofibers. At higher CNFs ratio, the presence of aggregated nanofibers seems to break up the KB branches and then the hybrid suspensions lose their electrical conductivity.

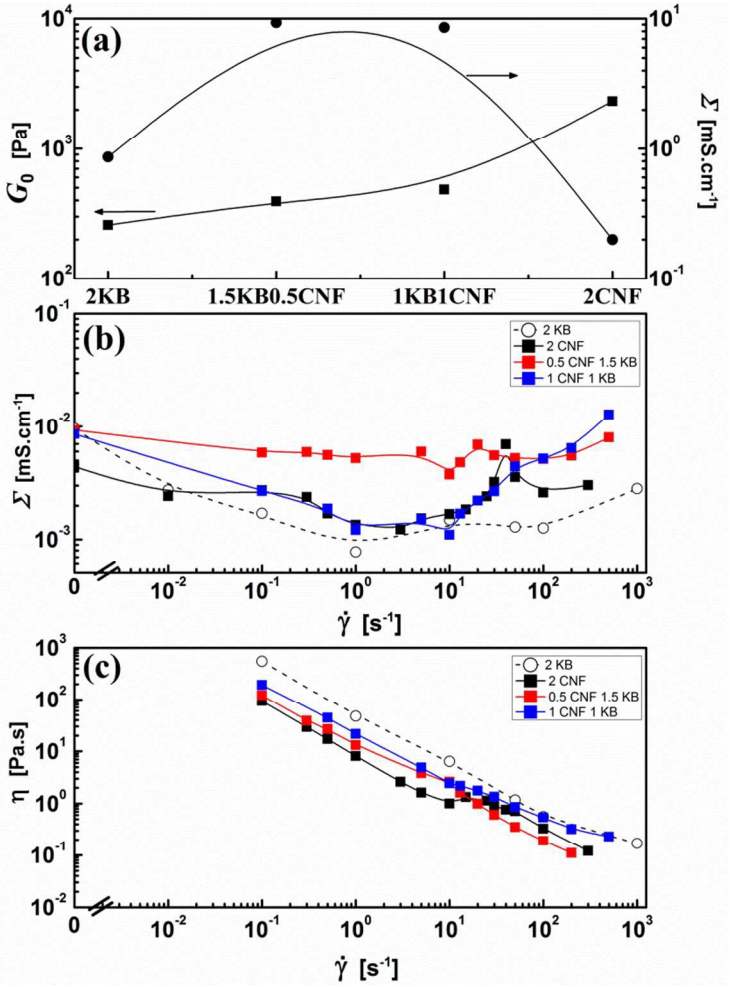

Fig. 8. Rheological and rheo-electrical properties of CNF-KB mixed carbons represented by the variation of plateau modulus and electrical conductivity with the carbon concentration (a), and the effect of shear rate on the steady shear viscosity (b) and electrical conductivity of the suspensions (c). The concentration of carbon materials is represented by wt% (e.g. 1.5KB0.5CNF denotes 1.5 wt% KB and 0.5 wt% CNFs, etc).

Figure 8b displays the variation of electrical conductivity of the suspensions of KB-CNFs mixed carbons under shear flow. It can be seen that the conductivity-shear rate curves have inverted bell-like shape with pronounced minima in accordance with a previous study.[5] This trend is linked to a structural transition under shear flow where the network of highly structured

suspensions breaks up at low shear rate so that the conductivity drops then the formation of large anisometric aggregates (at moderate shear rate) and small aggregates with high density of effective chains (at higher shear rate) again increases the conductivity of suspensions.[5] However, the suspension at 0.5 wt% CNFs + 1.5 wt% KB shows conductivity nearly independent of the shear rate. This may imply that the flexible "non-aggregated" nanofibers, at small amount of CNFs, simply wires the broken KB aggregates under flow[6] so that the conductivity does not alter in contrast to suspensions at higher CNFs content (1 wt%) where the aggregated nanofibers have a synergetic effect with the KB aggregates which are sensitive to shear flow.

The shear-induced structural transition can be also interpreted from the steady viscosity-shear rate curves as depicted in Figure 8c. Except for the 2 wt% KB,[91] the suspensions exhibit three-regime flow curves: two shear-thinning regimes at low and high shear rates separated with shear-thickening region at moderate shear rate in agreement with reported systems.[5,6,75,92] Such thickening region is more pronounced for pure 2 wt% CNFs and gradually diminishes as the KB ratio increases suggesting that the shape and size of aggregates are closely connected with the overall flow behavior of the suspensions.

Conclusion

The rheo-electrical measurements efficiently accounted for the equilibrium microstructure and shear-induced transition exhibited by suspensions of carbon nanofibers (CNFs) in an organic electrolyte (1 M lithium bis(trifluoromethanesulfonaimide) in propylene carbonate). Such nonaqueous conductive suspensions are precursor formulation for electrodes in energy storage systems such as redox flow batteries.

Over wide CNFs concentration, the suspensions commonly exhibited gel-like viscoelastic response with coincide rheological and electrical percolation threshold at ϕ=0.0068. This threshold separates two different networks: entangled- and aggregated-based structures controlled, respectively, by diffusion-limited aggregation (DLA) and reaction-limited aggregation (RLA) mechanisms. Both types of networks showed a three-regime flow curve (viscosity vs. shear rate) in agreement with inverted-bell-like conductivity curve (electric conductivity vs. shear rate) indicating shear-induced alignments (for the entangled network) and structural (for the aggregated network) transitions.

Owing to different particle morphology and hence aggregation mechanisms, the suspensions of anisometric CNFs showed higher rigidity than those of isometric carbon black (CB) in the same electrolyte. In contrary, the CB suspensions presented higher electric conductivity than that of their analogous CNFs as a consequence of aggregated-based network of

the CNFs where the electric current likely only flows in the outermost linked fibers rather than the aggregates (bundles). Hybrid suspension of CNFs and CB at an optimum mixing ratio resulted in an enhanced electric conductivity with nearly no influence on the suspension rigidity and on their electric conductivity under shear flow.

References

1 K. Tatsumi, K. Zaghib, Y. Sawada, H. Abe, T. Ohsaki, *J. Electrochem. Soc.*, 1995, **142**, 1090.
2 J. Liu, K. Tang, K. Song, P. A. van Aken, Y. Yu, J. Maier, *Phys. Chem. Chem. Phys.*, 2013, **15**, 20813.
3 M. Endo, Y. A. Kim, T. Hayashi, K. Nishimura, T. Matusita, K. Miyashita, M. S. Dresselhaus, *Carbon*, 2001, **39**, 1287.
4 C. Kim, K. S. Yang, M. Kojima, K. Yoshida, Y. J. Kim, Y. A. Kim, M. Endo, *Adv. Funct. Mater.*, 2006, **16**, 2393.
5 M. Youssry, L. Madec, P. Soudan, M. Cerbelaud, D. Guyomard, B. Lestriez, *Phys. Chem. Chem. Phys.*, 2013, **15**, 14476.
6 M. Youssry, L. Madec, P. Soudan, M. Cerbelaud, D. Guyomard, B. Lestriez, *J. Power Sources*, 2015, **274**, 424.
7 M. Inagaki, H. Konno, O. Tanaike, *J. Power Sources*, 2010, **195**, 7880.
8 A. V. Melechko, V. I. Merkulov, T. E. McKnight, M. A. Guillorn, K. L. Klein, D. H. Lowndes, M. L. Simpson, *J. Appl. Phys.*, 2005, **97**, 041301.
9 B. K. Ku, M. S. Emery, A. D. Maynard, M. R. Stolzenburg, P. H. McMurry, *Nanotechnology*, 2006, **17**, 3613.
10 L. A. Girifalco, M. Hodak, R. S. Lee, *Phys. Rev. B*, 2000, **62**, 13104.
11 H. Stahl, J. Appenzeller, R. Martel, P. Avouris, B. Lengeler, *Phys. Rev. Lett.*, 2000, **85**, 5186.
12 B. Vigolo, A. Pénicaud, C. Coulon, C. Sauder, R. Pailler, C. Journet, P. Bernier, P. Poulin, *Science*, 2000, **290**, 1331.
13 V. C. Moore, M. S. Strano, E. H. Haroz, R. H. Hauge, R. E. Smalley, J. Schmidt, Y. Talmon, *Nano Lett.*, 2003, **3**, 1379.
14 L. Calvillo, M. J. La´zaro, I. Suelves, Y. Echegoyen, E. G. Bordeje´, R. Moliner, *J. Nanosci. Nanotechnol.*, 2009, **9**, 4164.
15 N. T. Hung, N. M. Tuong, E. G. Rakov, *Inorg. Mater.*, 2010, **46**, 1077.
16 V. Datsyuk, M. Kalyva, K. Papagelis, J. Parthenios, D. Tasis, A. Siokou, I. Kallitsis, C. Galiotis, *Carbon*, 2008, **46**, 833.
17 K. Shen, H. Xu, Y. Jiang, T. Pietraß, *Carbon*, 2004, **42**, 2315.
18 S. C. Mun, M. Kim, K. Prakashan, H. J. Jung, Y. Son, O. O. Park, *Carbon*, 2014, **67**, 64.
19 A. Celzard, E. McRae, C. Deleuze, M. Dufort, G. Furdin, J. F. Marêché, *Phys. Rev. B*, 1996, **53**, 6209.
20 C. Penu, G.-H. Hu, A. Fernandez, P. Marchal, L. Choplin, *Polym. Eng. Sci.*, 2012, **52**, 2173.
21 J. N. Coleman, S. Curran, A. B. Dalton, A. P. Davey, B. McCarthy, W. Blau, R. C. Barklie, *Phys. Rev. B*, 1998, **58**, R7492.
22 L. Madec, M. Youssry, M. Cerbelaud, P. Soudan, D. Guyomard, B. Lestriez, *J. Electrochem. Soc.*, 2014, **161**, A693.
23 E. Anczurowski, R. G. Cox, S. G. Mason, J. Colloid Interface Sci., 1967, 23, 533.
24 M . H. Al-Saleh, U. Sundararaj, *Carbon*, 2009, **47**, 2.
25 K. Hyun, S. H. Kim, K. H. Ahn, S. J. Lee, *J. Non-Newtonian Fluid Mech.*, 2002, **107**, 51.
26 M. Youssry, L. Coppola, I. Nicotera, C. Morán, *J. Colloid Interface Sci.*, 2008, **321**, 459.
27 I. A. Kinloch, S. A. Roberts, A. H. Windle, *Polymer*, 2002, **43**, 7483.
28 L. A. Hough, M. F. Islam, P. A. Janmey, A. G. Yodh, *Phys. Rev. Lett.*, 2004, **93**, 168102.
29 F. C. MacKintosh, J. Käs, P. A. Janmey, *Phys. Rev. Lett.*, 1995, **75**, 4425.
30 R. Tharmann, M. M. A. E. Claessens, A. R. Bausch, *Phys. Rev. Lett.*, 2007, **98**, 088103.

31 S. S. Rahatekar, K. K. Koziol, S. R. Kline, E. K. Hobbie, J. W. Gilman, A. H. Windle, *Adv. Mater.*, 2009, **21**, 874.
32 Th. F. Tadros, Rheology of Dispersions: Principles and Applications, Wiley-VCH Verlag GmbH & Co. KGaA, Weinheim, 2010.
33 M. Kawaguchi, M. Okuno, T. Kato, *Langmuir*, 2001, **17**, 6041.
34 V. Grenard, N. Taberlet, S. Manneville, *Soft Matter*, 2011, **7**, 3920.
35 E. K. Hobbie, D. J. Fry, *J. Chem. Phys.*, 2007, **126**, 124907.
36 K. M. Yearsley, M. R. Mackley, F. Chinesta, A. Leygue, *J. Rheol.*, 2012, **56**, 1465.
37 E. E. Urenà-Benavides, M. J. Kayatin, V. A. Davis, *Macromolecules*, 2013, **46**, 1642.
38 J. Xu, S. Chatterjee, K. W. Koelling, Y. Wang, S. E. Bechtel, *Rheol. Acta*, 2005, **44**, 537.
39 R. Larson, The Structure and Rheology of Complex Fluids, Oxford University Press, 1999.
40 A. W. K. Ma, M. R. Mackley, F. Chinesta, *Int. J. Mater. Form.*, 2008, **1**, 75.
41 Z. H. Fan, S. G. Advani, *J. Rheol.*, 2007, **51**, 585.
42 M.-C. Yang, L. E. Scriven, C. W. Macosko, *J. Rheol.*, 1986, **30**, 1015.
43 O. Lieleg, M. M. A. E. Claessens, C. Heussinger, E. Frey, A. R. Bausch, *Phys. Rev. Lett.*, 2007, **99**, 088102.
44 S. Marceau, Ph. Dubois, R. Fulchiron, Ph. Cassagnau, *Macromolecules*, 2009, **42**, 1433.
45 W.-H. Shih, W. Y. Shih, S.-I. Kim, J. Liu, I. A. Aksay, *Phys. Rev. A*, 1990, **42**, 4772.
46 H. Wu, M. Morbidelli, *Langmuir*, 2001, **17**, 1030.
47 In the strong-link regime, D is expected to fall in the range of 1.7-2.0 [46]. Accordingly the exponent of G_0 power law relation (Eq. 1) will yield negative x values (x= -0.27 and -0.90) which cannot be explained by the scaling model [45] and has been found in some colloidal suspensions [49].
48 F. Khalkhal, P. J. Carreau, G. Ausias, *J. Rheol.*, 2011, **55**, 153.
49 F. Khalkhal, P. J. Carreau, *Rheol. Acta*, 2011, **50**, 717.
50 N. B. Uriev, I. Y. Ladyzhinsky, *Colloids Surfaces A*, 1996, **108**, 1.
51 K.-M. Jäger, D. H. McQueen, *Polymer*, 2001, 42, 9575.
52 P. Meakin, *Phys. Rev. Lett.*, 1983, **51**, 1119.
53 M. Kolb, R. Botet, R. Jullien, *Phys. Rev. Lett.*, 1983, **51**, 1123.
54 D. Stauffer, A. Aharony, Introduction to Percolation Theory, Taylor & Francis, London, 1994.
55 F. Du, R. C. Scogna, W. Zhou, S. Brand, J. E. Fischer, K. I. Winey, *Macromolecules*, 2004, **37**, 9048.
56 G. Hu, C. Zhao, S. Zhang, M. Yang, Z. Wang, *Polymer*, 2006, **47**, 480.
57 F. M. Blighe, Y. R. Hernandez, W. J. Blau, J. N. Coleman, *Adv. Mater.*, 2007, **19**, 4443.
58 I. Alig, T. Skipa, D. Lellinger, P. Pötschke, *Polymer*, 2008, **49**, 3524.
59 O. Meincke, D. Kaempfer, H. Weickmann, C. Friedrich, M. Vathauer, H. Warth, *Polymer*, 2004, **45**, 739.
60 Q. Zhang, D. R. Lippits, S. Rastogi, *Macromolecules*, 2006, **39**, 658.
61 J. Sumfleth, S. T. Buschhorn, K. Schulte, *J. Mater. Sci.*, 2011, **46**, 659.
62 M. D. Lima, M. J. Andrade, V. Skakalova, C. P. Bergmann, S. Roth, *J. Mater. Chem.*, 2007, **17**, 4846.
63 C. Penu, G.-H. Hu, A. Fernandez, Ph. Marchal, L. Choplin, *Polym. Eng. Sci.*, 2012, **52**, 2173.
64 V. Skakalova, U. Dettlaff-Weglikowska, S. Roth, *Synth. Met.*, 2005, **152**, 349.
65 S. Mall, W. B. Russel, *J. Rheol.*, 1987, **31**, 651.
66 T. Amari, K. Watanabe, *J. Rheol.*, 1990, **34**, 207.

67 L. Vaisman, H. D. Wagner, G. Marom, *Adv. Colloid Interface Sci.*, 2006, **128–130**, 37.
68 In tandem with the variation of G_0 and σ_y with the nanofibers volume fraction (Fig. 4), the steady viscosity η (at 0.1 s^{-1}) similarly shows three-regime dependence of the volume fraction with different exponents indicating different microstructure. (**Fig. S-2**).
69 V. A. Davis, L. M. Ericson, A. N. G. Parra-Vasquez, H. Fan, Y. Wang, V. Prieto, J. A. Longoria, S. Ramesh, R. K. Saini, C. Kittrell, W. E. Billups, W. .W. Adams, R. H. Hauge, R. E. Smalley, M. Pasquali, *Macromolecules*, 2004, **37**, 154.
70 A. Zaccone, D. Gentili, H. Wu, M. Morbidelli, E. Del Gado, *Phys. Rev. Lett.*, 2011, **106**, 138301.
71 X. Sha, K. Yu, H. Cao, K. Qian, *J. Nanopart. Res.*, 2013, **15**, 1816.
72 G. Natale, M. C. Heuzey, P. J. Carreau, G. Ausias, J. Férec, *AIChE J.*, 2014, **60**, 1476.
73 N. J. Wagner, J. F. Brady, *Phys. Today*, 2009, **62**, 27.
74 D. P. Kalman, N. J. Wagner, *Rheol. Acta*, 2009, **48**, 897.
75 C. O. Osuji, C. Kim, D. A. Weitz, *Phys. Rev. E*, 2008, **77**, 060402.
76 A. S. Negi, C. O. Osuji, *Rheol. Acta*, 2009, **48**, 871.
77 S. Lin-Gibson, J. A. Pathak, E. A. Grulke, H. Wang, E. K. Hobbie, *Phys. Rev. Lett.*, 2004, **92**, 048302.
78 E. K. Hobbie, *Rheol. Acta*, 2010, **49**, 323.
79 E. Brown, H. M. Jaeger, *J. Rheol.*, 2012, **56**, 875.
80 K. L. White, P. Li, Y. Sumi, H.-J. Sue, *J. Phys. Chem. B*, 2014, **118**, 362.
81 L. Madec, M. Youssry, M. Cerbelaud, P. Soudan, D. Guyomard, B. Lestriez, *ChemPlusChem*, 2015, **80**, 396.
82 S. Pujari, S. S. Rahatekar, J. W. Gilman, K. K. Koziol, A. H. Windle, W. R. Burghardt, *J. Chem. Phys.*, 2009, **130**, 214903.
83 S. B. Kharchenko, J. F. Douglas, J. Obrzut, E. A. Grulke, K. B. Migleri, *Nat. Mater.*, 2004, **3**, 564.
84 A. E. Eken, E. J. Tozzi, D. J. Klingenberg, W. Bauhofer, *Polymer*, 2011, **52**, 5178.
85 Y. Aoki, A. Hatano, H. Watanabe, *Rheol. Acta*, 2003, **42**, 209.
86 C. L. Barrie, P. C. Griffiths, R. J. Abbott, I. Grillo, E. Kudryashov, C. Smyth, *J. Colloid Interface Sci.*, 2004, **272**, 210.
87 T. Kitano, T. Kataoka, T. Shirota, *Rheol. Acta*, 1981, **20**, 207.
88 L. M. Clingerman, E. H. Weber, J. A. King, K. H. Schulz, *Polym. Compos.*, 2002, **23**, 911.
89 W. Thongruang, R. J. Spontak, C. M. Balik, *Polymer*, 2002, **43**, 2279.
90 M. Drubetski, A. Siegmann, M. Nakis, *J. Mater. Sci.*, 2007, **42**, 1.
91 The 2 wt% KB suspension does not show a clear shear-thickening region due to the formation of small and somewhat monodisperse hydroclusters which interact enough strong to have a higher yield stress [5] leading to masking the shear-thickening [E. Brown, N. A. Forman, C. S. Orellana, H. Zhang, B. W. Maynor, D. E. Betts, J. M. DeSimone, H. M. Jaeger, *Nat. Mater.*, 2010, **9**, 220].
92 B. J. Maranzano, N. J. Wagner, *J. Chem. Phys.*, 2001, **114**, 10514.